

# Transverse Demagnetization Dynamics of a Unitary Fermi Gas

A. B. Bardon<sup>1</sup>, S. Beattie<sup>1</sup>, C. Luciuk<sup>1</sup>, W. Cairncross<sup>1</sup>, D. Fine<sup>1</sup>, N. S. Cheng<sup>1</sup>,  
G. J. A. Edge<sup>1</sup>, E. Taylor<sup>2</sup>, S. Zhang<sup>3</sup>, S. Trotzky<sup>1</sup>, J. H. Thywissen<sup>1,4</sup>

<sup>1</sup> *Department of Physics, CQIQC, and Institute for Optical Sciences, University of Toronto, M5S 1A7 Canada*

<sup>2</sup> *Department of Physics and Astronomy, McMaster University, L8S 4M1 Canada*

<sup>3</sup> *Department of Physics, Center of Theoretical and Computational Physics, University of Hong Kong, China and*

<sup>4</sup> *Canadian Institute for Advanced Research, Toronto, Ontario, M5G 1Z8 Canada*

(Dated: January 27, 2023)

Understanding the quantum dynamics of strongly interacting fermions is a challenge raised by diverse forms of matter, including high-temperature superconductors, neutron stars, and quark-gluon plasmas. An appealing benchmark is offered by cold atomic gases in the unitary limit of strong interactions, where the system is both scale-invariant and known to obey universal thermodynamics in equilibrium. Here we study the dynamics of a transversely magnetized unitary Fermi gas in an inhomogeneous magnetic field. We find that demagnetization is caused by diffusive spin transport with a diffusion constant that saturates at low temperatures to the conjectured quantum-mechanical lower bound  $\simeq \hbar/m$ , where  $m$  is the particle mass. The development of pair correlations is observed by measuring Tan's contact parameter.

Short-range interactions reach their quantum-mechanical limit when the scattering length that characterizes inter-particle collisions diverges. The absence of a small parameter in this *unitary* regime renders a quantitative and sometimes even a qualitative theoretical description challenging. A well controlled model system that realizes unitarity is provided by ultracold fermionic alkali atoms tuned to a Fano-Feshbach resonance [1]. These scale-invariant gases are characterized by universal parameters not only relevant to all species of cold atoms in this limit, but also, for example, to the crust of neutron stars at twenty-five orders of magnitude higher density [2, 3]. While experiments with ultracold atoms have already greatly contributed to the understanding of equilibrium properties of unitary gases [4–6], the nature of transport in this extreme form of matter so far remains elusive. Recent measurements provide a glimpse into unitary non-equilibrium dynamics and spin transport properties [7–10]. Here, we measure the demagnetization dynamics of an initially fully spin-polarized, ideal Fermi gas with two available resonantly interacting spin eigenstates in a three-dimensional (3D) geometry. The loss of magnetization is driven by a magnetic field gradient and transverse spin diffusion and imposes a drastic transformation of the non-interacting gas toward a unitary spin mixture. We follow the complex many-body dynamics by time-resolved measurements of both the bulk magnetization and emerging local pair correlations.

Spin diffusion is the transport phenomenon that relaxes magnetic inhomogeneities in a many-body system. At low temperature, where Pauli blocking can suppress collision rates, one must distinguish between diffusion driven by gradients either in the magnitude of magnetization (*longitudinal*) or in its direction (*transverse* spin diffusion), quantified by individual diffusivities  $D_s^{\parallel}$  and  $D_s^{\perp}$ , respectively [11, 12]. Within the kinetic theory of

transport, spin current is carried by some quasi-particle with kinetic energy  $\epsilon$  and lifetime  $\tau_{qp}$ . The diffusion constant is then  $\sim \epsilon\tau_{qp}/m$ . In the unitary regime, strong scattering can drastically reduce  $\tau_{qp}$ , challenging the self-consistency of the kinetic picture when  $\tau_{qp}$  approaches the Heisenberg limit  $\hbar/\epsilon$ , at which the diffusivity reaches its quantum-mechanical lower bound  $\sim \hbar/m$ . A measurement of the longitudinal diffusivity  $D_s^{\parallel}$  in 3D yielded a minimum trap-averaged value of  $\simeq 6.3\hbar/m$ , which is consistent with the Heisenberg bound after compensating for inhomogeneities [9, 13]. More recently, a transverse diffusivity two orders of magnitude smaller than  $\hbar/m$  was observed in a strongly interacting two-dimensional (2D) Fermi gas [10, 14]. In our experiments, we find a lower bound for  $D_s^{\perp}$  in a 3D unitary Fermi gas that is remarkably close to  $\hbar/m$ , demonstrating a universal lower limit of diffusive spin transport for the 3D unitary gas.

All of our measurements are carried out with samples of ultracold <sup>40</sup>K atoms. Each atom is prepared in an equal superposition of two resonantly interacting inter-

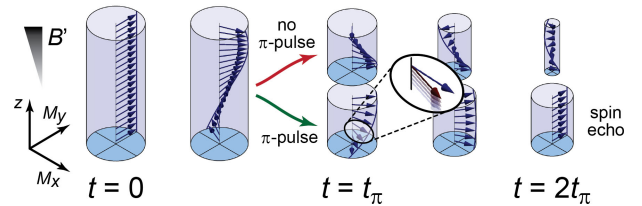


FIG. 1. **Magnetization dynamics.** A  $\pi/2$  pulse at  $t = 0$  initializes the system with a homogeneous magnetization ( $M_y = 1$  in the rotating frame) perpendicular to the magnetic field, which is along  $z$ . A spin spiral develops because of a magnetic field gradient, and drives diffusive spin currents (zoom ellipse). The upper and lower sequences show evolution without and with a  $\pi$  pulse, respectively.

nal states, labeled  $|\uparrow\rangle$  and  $|\downarrow\rangle$  [14], which corresponds to a gas with full transverse magnetization  $M_y = 1$  [Fig. 1]. We use two states that block any local mechanism for magnetization relaxation, unlike the scenario typical of condensed matter. However, their difference in magnetic moment  $\Delta\mu$  allows an applied magnetic field gradient  $B' = \partial B/\partial z$  to twist the spin into a spiral pattern, leading to a gradient in transverse magnetization. This gradient drives diffusive spin transport that erodes the coherence irreversibly. The evolution of transverse magnetization  $M_\perp = M_x + iM_y$  is modeled with  $\partial_t M_\perp = -i\alpha z M_\perp + D_s^\perp \nabla^2 M_\perp$ , where  $\alpha = \Delta\mu B'/\hbar$  [15]. This equation is solved by  $M_\perp(\vec{r}, t) = i \exp[-i\alpha z t - t^3/6\tau^3]$ , where

$$\tau = (2D_s^\perp \alpha^2)^{-1/3} \quad (1)$$

is the time constant of demagnetization and a measure of  $D_s^\perp$ . Since there is no spatial gradient in the magnetization amplitude, the dynamics do not probe  $D_s^\parallel$ .

The effect of spin diffusion on magnetization is measured using a spin-echo technique [Fig. 1]. A spin-refocusing  $\pi$ -pulse at time  $t_\pi$  swaps the population of the states  $|\uparrow\rangle$  and  $|\downarrow\rangle$ , which causes the spin spiral to untwist at  $t = 2t_\pi$ , leaving a homogeneous magnetization  $M_\perp(t) = -i \exp[-t^3/24\tau^3]$ . The final cloud-averaged  $|M_\perp|$  is indicated by the contrast in  $|\uparrow\rangle$  and  $|\downarrow\rangle$  after a final  $\pi/2$  pulse with variable phase [14].

Starting with an initial temperature of  $(T/T_F)_i = 0.25(3)$ , where  $T_F$  is the Fermi temperature of the spin-polarized gas at  $t = 0$ , we observe that the magnetization at the echo time is well fit by  $\exp[-(t/\tau_M)^3]$  [see inset in Fig. 2(a)]. The time constant  $\tau_M$  is typically on the millisecond scale for our parameters. We further test the model by extracting  $\tau = \tau_M/24^{1/3}$  across a wide range of gradients, and find the predicted  $(B')^{-2/3}$  scaling [Fig. 2(a)]. A single-parameter fit of equation (1) to the data yields  $D_s^\perp = (1.08 \pm 0.09^{+0.17}_{-0.13}) \hbar/m$ , where the uncertainties are the statistical error from the fit and the systematic error from the gradient calibration, respectively. This is a direct measurement of the trap-averaged diffusivity which does not rely on knowledge of cloud size, density, trap frequencies, or any calibration other than that of the gradient.

In Figure 2(b), we choose a constant gradient and vary  $(T/T_F)_i$ . As above, we interpret the observed magnetization decay time  $\tau_M$  as a measure of  $D_s^\perp$ . We find demagnetization to decay faster at higher initial temperatures, corresponding to larger values of  $D_s^\perp$ . This is expected, since the typical kinetic energy scales as  $T$  while the collisional lifetime scales as  $T^2$  for fixed atom number and trap parameters at unitarity. Remarkably, we find  $D_s^\perp$  to be bounded from below by  $\simeq \hbar/m$  and that this bound is saturated in the vicinity of  $(T/T_F)_i = 0.25$ . At lower temperatures, we find deviations from the cubic magnetization decay, i. e. a more rapid decay at lower magnetization. Such a behavior is predicted to occur below

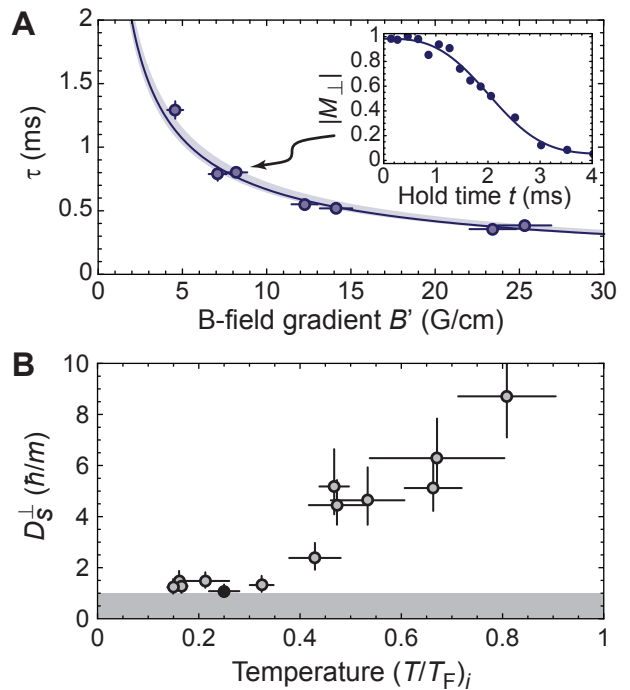


FIG. 2. **Spin diffusion.** (a) Magnetization decay times  $\tau$  at various gradients. Horizontal and vertical error bars reflect the systematic error in the gradient calibration and the fit error respectively. The solid line is a single-parameter fit of equation (1) to the data, and the shaded area denotes the combined statistical and systematic uncertainty. The inset shows a sample of  $|M_\perp(t)|$  at  $B' = 8.2(7)$  G/cm with a fit using the spin-diffusion model (solid line). (b) Measured  $D_s^\perp$  for various initial temperatures at a single gradient  $B' = 18(1)$  G/cm. To achieve temperature control, the data was collected with  $N_{\text{Total}} = 1 \dots 7 \times 10^4$ . The filled circle marks the diffusivity obtained from the data in (a) at  $(T/T_F)_i = 0.25(3)$  and the shaded area covers  $D_s^\perp < \hbar/m$ .

the so-called anisotropy temperature, where  $D_s^\perp$  becomes magnetization dependent and also  $D_s^\perp$  and  $D_s^\parallel$  differ significantly [12, 16]. It can also arise from spin rotation effects [17, 18] and our current measurement protocol is not suitable to distinguish between the two possibilities.

During demagnetization, the system transforms from having a single Fermi surface with  $N_{\text{Total}}$  particles and Fermi energy  $E_{F,i}$  to having two spin populations in diffusive equilibrium, each with  $N = N_{\text{Total}}/2$  atoms. The final Fermi energy  $E_{F,f}$  therefore is reduced by a factor of  $2^{1/3}$  compared to  $E_{F,i}$ . Furthermore, the relaxation of the Fermi surfaces as well as the release of attractive interaction energy leads to a rise in temperature. Each measurement of  $D_s^\perp$  then has to be understood as a time average over a range in temperature, as well as an average over the local reduced temperature across the trap. The intrinsic heating together with the initial polarization of the cloud ensures that the gas remains in the normal phase throughout the evolution [19].

While our result for the transverse spin diffusivity reflects the suppression of transport by strong scattering, it does not reveal how interactions emerge in the many-body system. In a complementary set of measurements, we study the microscopic transformation of the gas by following the dynamical evolution of pair correlations that is enabled by demagnetization. Instead of the final  $\pi/2$  pulse, the gas is probed at time  $t$  by a  $20\ \mu\text{s}$  radiofrequency (rf) pulse coupling the  $|\uparrow\rangle$  state to an initially unoccupied internal state  $|p\rangle$  that interacts only weakly with  $|\uparrow\rangle$  and  $|\downarrow\rangle$ . The transfer rate to  $|p\rangle$  is measured as a function of the frequency detuning  $\delta$  above the single-particle resonance. In a strongly interacting gas in equilibrium, the high-frequency tail of such a spectrum is known to be proportional to Tan's contact parameter  $C = \int d\mathbf{r} \mathcal{C}(\mathbf{r})$ , and scales as  $\delta^{-3/2}$  [20–27]. The contact density  $\mathcal{C}(\mathbf{r}) = \langle g^2 \psi_\uparrow^\dagger(\mathbf{r}) \psi_\downarrow^\dagger(\mathbf{r}) \psi_\downarrow(\mathbf{r}) \psi_\uparrow(\mathbf{r}) \rangle$  is a local measure of the pair correlation, i.e., the number of pairs of opposite spins at short distance, where  $g$  is the coupling constant and  $\psi_\sigma$  is the annihilation operator with spin  $\sigma$ . As is clear from its definition,  $C$  is also proportional to the interaction energy. Although contact has been shown to relate various thermodynamic and many-body properties of a short-range interacting gas, it has so far been studied only in equilibrium and with an unmagnetized gas [23, 27, 28].

Figure 3(a) shows that after a short hold time the spectrum exhibits only the single-particle peak, while after a longer hold time, the spectrum develops a high-frequency tail. Whenever a high-frequency tail is observed, we find that it has a  $\delta^{-3/2}$  scaling at  $\delta \gtrsim 4E_{F,f}/\hbar$ , indicating that pair correlations can be described with a contact parameter throughout the dynamics [Fig. 3(b)].

Figure 4(a) shows that, under various protocols, the contact starts at zero and grows in time towards a maximal value of  $C_{\text{max}}/(k_F N) = 1.53(4)$ , where  $\hbar k_F = \sqrt{2mE_{F,f}}$  is the Fermi momentum in the final state and  $N$  is the number of atoms per spin state. This is comparable to equilibrium values observed previously at  $T/T_F \simeq 0.35$  in Ref. 28, which lies between the initial and final temperatures of this data. At longer times ( $t > 5$  ms), Figure 4(a) shows a slow reduction of contact, which is likely due to heating; however, in this work we focus on the short-time dynamics. A fit using an empirical rise function  $f(t) = C_{\text{max}}(1 - \exp[-(t/\tau_C)^\eta])$  to the short-time data yields an exponent of  $\eta = 3.6(3)$  with a spin-reversal and  $\eta = 2.8(2)$  without a spin-reversal, reminiscent of the magnetization loss function  $\propto \exp[-(t/\tau_M)^3]$ . Further connection of contact to magnetization is demonstrated by Figure 4(b), which traces the contact during a spin-reversal sequence: the rise of  $C/(k_F N)$  is slowed by the refocusing pulse and plateaus at the spin-echo time, around which transverse spin diffusion is suppressed.

Figure 4(c) compares the  $1/e$  time scales of magnetization loss,  $\tau_M$ , and contact rise,  $\tau_C$ , with and without an echo. A linear relationship is found, which is sur-

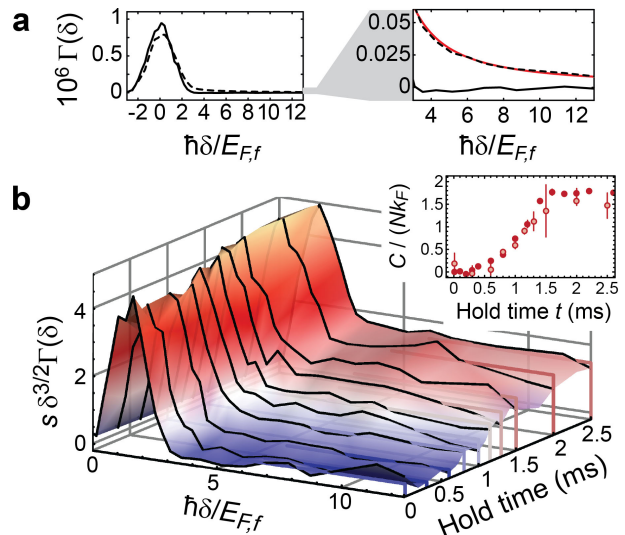


FIG. 3. **Time-resolved spectroscopy to measure Tan's contact.** (a) Rf spectra for  $t = 10\ \mu\text{s}$  (solid line) and  $2.5\ \text{ms}$  (dashed line), both without a spin-refocusing pulse. The red line in the right panel is a fit of a power-law  $\propto \delta^{-3/2}$  to the high-frequency tail for  $t = 2.5\ \text{ms}$ . (b) Rf spectra multiplied with  $s\delta^{3/2}$  versus hold time, where  $s \equiv \pi^2(2\hbar/E_{F,f})^{3/2}$ , revealing a plateau for large positive detunings  $\delta \gtrsim 4E_{F,f}/\hbar$ . The inset compares contact values extracted from these full spectra (open circles) and those measured at a fixed detuning  $\delta/2\pi = 125\ \text{kHz}$  (filled circles). The latter method allows single-shot study of contact dynamics, and thus reduced statistical noise as seen here. Error bars in (b) are statistical.

prising at first, since magnetization is a one-body vector observable and contact is a two-body scalar observable. The connection comes from the Pauli exclusion principle, which requires that if two particles are in the same location, as is required for a contact interaction, their spin state must be the antisymmetric spin-singlet state. For *uncorrelated* spin pairs, the probability to be in a spin-singlet state is  $\rho_{ss} = (1 - |M_\perp|^2)/4$ . Combining this assumption with the diffusion model for magnetization predicts  $\tau_C = \tau_M/2^{1/3}$  and  $\tau_C = \tau_M/2$  with and without an echo, respectively. The *maximum* singlet probability for a given magnetization is  $\rho_{ss} = 1 - |M_\perp|$ , and would instead give  $\tau_C/\tau_M$  that is  $2^{1/3}$  larger. Data in Figure 4(c) show an approximately linear relation whose slope is between these two limits.

Comparing the full range of measured values for normalized  $C$  and  $|M_\perp|$  at various times and gradients in Figure 4(d) also shows a functional form between the uncorrelated  $C \sim 1 - |M_\perp|^2$  and the fully paired  $C \sim 1 - |M_\perp|$ . A calculation based on a large- $\mathcal{N}$  expansion predicts that  $C(M_\perp)$  changes between these limiting behaviors as  $T$  goes from  $2T_c$  to  $T_c$ , where  $T_c$  is the critical temperature for pair superfluidity [14]. Since a singlet pair has no net spin, the observation of enhanced  $\rho_{ss}$  is

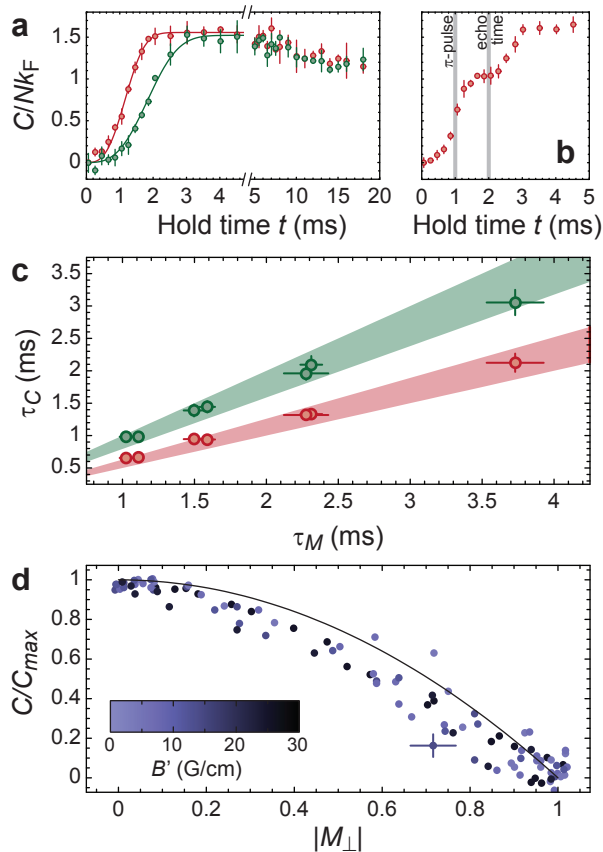


FIG. 4. **Linking contact and magnetization.** The time evolution of contact is studied using single-shot spectroscopy as described in Figure 3(b), at  $B' = 8.2(7)$  G/cm. (a) Contact versus hold time  $t$  with (in green) and without (in red) a spin-refocusing  $\pi$  pulse at  $t/2$ . Solid lines show cubic ( $\eta = 3$ ) fits to the data as described in the text. (b) Contact versus hold time  $t$  with a  $\pi$  pulse applied at  $t_\pi = 1$  ms. At the echo time, the spin spiral has untwisted and no longer drives a diffusive spin current. Error bars in (a) and (b) show statistical error across repeated measurements. (c) Contact growth time,  $\tau_C$ , versus demagnetization time,  $\tau_M$  (colors as in (a)), measured at various gradients  $B'$ . Shaded areas interpolate between the limits of fully paired and uncorrelated spins. (d) Normalized contact versus magnetization obtained by relating measurements of  $|M_\perp(t)|$  and  $C(t)$  for all sampled gradients  $B'$ . The solid line shows the prediction for uncorrelated spins (see text). A typical statistical error bar is shown on a single point.

also consistent with prior observations of reduced magnetic susceptibility due to strong attractive interactions in the normal state [29, 30].

Alternatively, an apparent reduction in  $C(M_\perp)$  might arise from a lag in the evolution of  $C$  behind  $|M_\perp|$ . However we find no statistically significant dependence on gradient, which is evidence for a quasi-equilibrium of  $C$  during demagnetization. A true steady-state transport measurement, on the other hand, would suffer from an

inhomogeneous magnetization due to imbalanced chemical potentials in the trap. Our dynamic measurement avoids this problem, since spin transport is strongly suppressed on the millisecond time scale [7, 9].

In conclusion, we have shown how a quantum-degenerate Fermi gas at an interaction resonance loses its magnetization and becomes strongly correlated. Our observation of a lower bound for the transverse spin diffusion constant of  $\simeq \hbar/m$  challenges the conventional paradigm of transport by implying the necessity of maximally incoherent quasiparticles. A similar limit to the quasiparticle lifetime would explain the ubiquitous  $T$ -linear resistivity in metals [31], and a quantum-limited viscosity [8]. We pioneer the study of contact dynamics, which in the presented case, are found to be driven by magnetization dynamics. We also show that the dynamical relation  $C(M)$  can be used to investigate singlet pairing in the normal state.

We thank B. Braverman, I. Kivlichan, L. LeBlanc, and T. Pfau for experimental assistance, D. DeMille, T. Enss, L. Jiang, A. Leggett, and A. Paramekanti for discussions, and A. Aspect for manuscript comments. S.T. acknowledges support from CQIQC. This work was supported by NSERC, CIFAR, AFOSR, and the University of Hong Kong.

- 
- [1] I. Bloch, J. Dalibard, and S. Nascimbène, *Nature Phys.* **8**, 267 (2012).
  - [2] G. A. Baker, *Phys. Rev. C* **60**, 054311 (1999).
  - [3] T.-L. Ho, *Phys. Rev. Lett.* **92**, 090402 (2004).
  - [4] S. Nascimbène, N. Navon, K. J. Jiang, F. Chevy, and C. Salomon, *Nature* **463**, 1057 (2010).
  - [5] M. Horikoshi, S. Nakajima, M. Ueda, and T. Mukaiyama, *Science* **327**, 442 (2010).
  - [6] M. J. Ku, A. T. Sommer, L. W. Cheuk, and M. W. Zwierlein, *Science* **335**, 563 (2012).
  - [7] Y. Liao, M. Reville, T. Paprotta, A. S. C. Rittner, W. Li, R. B. Partridge, and R. G. Hulet, *Phys. Rev. Lett.* **107**, 145305 (2011).
  - [8] C. Cao, E. Elliott, J. Joseph, H. Wu, J. Petricka, T. Schäfer, and J. E. Thomas, *Science* **331**, 58 (2011).
  - [9] A. Sommer, M. Ku, G. Roati, and M. W. Zwierlein, *Nature* **472**, 201 (2011).
  - [10] M. Koschorreck, D. Pertot, E. Vogt, and M. Köhl, *Nature Phys.* **9**, 405 (2013).
  - [11] A. Meyerovich, *Physics Letters A* **107**, 177 (1985).
  - [12] J. W. Jeon and W. J. Mullin, *Phys. Rev. Lett.* **62**, 2691 (1989).
  - [13] T. Enss and R. Haussmann, *Phys. Rev. Lett.* **109**, 195303 (2012).
  - [14] See supplementary material.
  - [15] A. Abragam, *The Principles of Nuclear Magnetism* (Oxford University Press, London, 1961).
  - [16] T. Enss, *Phys. Rev. A* **88**, 033630 (2013).
  - [17] A. J. Leggett, *J. Phys. C* **3**, 448 (1970).
  - [18] C. Lhuillier and F. Laloë, *J. Phys.-Paris* **43**, 225 (1982).
  - [19] M. W. Zwierlein, A. Schirotzek, C. H. Schunck, and

- W. Ketterle, *Science* **311**, 492 (2006).
- [20] S. Tan, *Ann. Phys.* **323**, 2952 (2008).
- [21] E. Braaten and L. Platter, *Phys. Rev. Lett.* **100**, 205301 (2008).
- [22] S. Zhang and A. J. Leggett, *Phys. Rev. A* **79**, 023601 (2009).
- [23] F. Werner and Y. Castin, *Phys. Rev. A* **86**, 013626 (2012), and references therein.
- [24] E. Braaten, D. Kang, and L. Platter, *Phys. Rev. Lett.* **104**, 223004 (2010).
- [25] W. Schneider and M. Randeria, *Phys. Rev. A* **81**, 021601 (2010).
- [26] P. Pieri, A. Perali, and G. C. Strinati, *Nature Phys.* **5**, 736 (2009).
- [27] J. T. Stewart, J. P. Gaebler, T. E. Drake, and D. S. Jin, *Phys. Rev. Lett.* **104**, 235301 (2010).
- [28] E. D. Kuhnle, S. Hoinka, P. Dyke, H. Hu, P. Hannaford, and C. J. Vale, *Phys. Rev. Lett.* **106**, 170402 (2011).
- [29] C. Sanner, E. J. Su, A. Keshet, W. Huang, J. Gillen, R. Gommers, and W. Ketterle, *Phys. Rev. Lett.* **106**, 010402 (2011).
- [30] S. Nascimbène, N. Navon, S. Pilati, F. Chevy, S. Giorgini, A. Georges, and C. Salomon, *Phys. Rev. Lett.* **106**, 215303 (2011).
- [31] J. A. N. Bruin, H. Sakai, R. S. Perry, and A. P. Mackenzie, *Science* **339**, 804 (2013).
- [32] C. A. R. Sá de Melo, M. Randeria, and J. R. Engelbrecht, *Phys. Rev. Lett.* **71**, 3202 (1993).
- [33] P. Nikolic and S. Sachdev, *Phys. Rev. A* **75** (2007).
- [34] M. Y. Veillette, D. E. Sheehy, and L. Radzihovsky, *Phys. Rev. A* **75** (2007).
- [35] T. Enss, *Phys. Rev. A* **86**, 013616 (2012).
- [36] S. Tan, *Ann. Phys.* **323**, 2971 (2008).
- [37] Z. Yu, G. M. Bruun, and G. Baym, *Phys. Rev. A* **80**, 023615 (2009).

## SUPPLEMENTARY MATERIAL

### SAMPLE PREPARATION

Fermionic, spin-polarized  $^{40}\text{K}$  atoms are cooled sympathetically with bosonic  $^{87}\text{Rb}$  atoms. Both species are initially trapped in a microfabricated magnetic trap, where  $^{87}\text{Rb}$  is evaporated directly. The final stage of cooling is performed in a crossed-beam optical dipole trap (ODT), with  $^{40}\text{K}$  atoms in the  $|F = 9/2, m_F = -9/2\rangle$  state and  $^{87}\text{Rb}$  atoms in the  $|F = 1, m_F = 1\rangle$  state. At the end of cooling, residual  $^{87}\text{Rb}$  atoms are removed with a resonant light pulse. The ODT has a mean frequency  $\bar{\omega}/2\pi = 486(15)$  Hz, and an aspect ratio of 4:1:1. The Feshbach field  $B_z$  and the gradient  $B' = \partial_z B_z$  are applied along a tight axis of the trap. The  $|\downarrow\rangle$ ,  $|\uparrow\rangle$ , and  $|p\rangle$  states in the main text refer to the high-field states adiabatically connected to the low-field  $m_F = -9/2, -7/2$ , and  $-5/2$  states of the  $F = 9/2$  hyperfine manifold of the electronic ground state.

The data shown in Figure 2(a) and Figure 4 was taken with  $N_{\text{Total}} = 3(1) \times 10^4$  atoms with an initial temperature of 330(30) nK. The initial Fermi temperature in these cases was  $T_{F,i} = E_{F,i}/k_B = 1.3(1) \mu\text{K}$ , resulting in  $(T/T_F)_i = 0.25(3)$ . The uncertainties stated for atom numbers and temperatures are a combination of statistical and calibration uncertainties. After complete demagnetization, the number of atoms per spin state is halved, to  $N_\sigma = N_{\text{Total}}/2$ , and the Fermi energy drops by  $2^{1/3}$  to  $E_{F,f}/k_B = 1.0(1) \mu\text{K}$ . This latter value, along with the corresponding  $k_F = \sqrt{2mE_{F,f}}/\hbar$ , is used in the normalization of the contact spectra.

In order to tune  $(T/T_F)_i$  for the measurements presented in Figure 2(b), we vary the loading and evaporation sequence, affecting both the absolute temperature of the gas and the total atom number. Spectroscopy data presented in Figure 3 was taken with higher atom number of  $N_{\text{Total}} \simeq 5 \times 10^4$  at  $(T/T_F)_i \simeq 0.2$  to enhance the signal-to-noise ratio.

### MAGNETIC FIELD CONTROL

We control the magnetic field and its gradients through a combination of magnetic field coils and microfabricated wires on an atom chip located about 200  $\mu\text{m}$  from the atoms. We tune the field to be  $|\mathbf{B}| = B_z = 202.10(2)$  G, at which the two states  $|\uparrow\rangle$  and  $|\downarrow\rangle$  undergo a Feshbach resonance. The field is calibrated by measuring the  $|\downarrow\rangle$  to  $|\uparrow\rangle$  transition frequency, which we find to be  $2\pi \times 44.817(4)$  MHz, and the uncertainty represents day-to-day fluctuation of the 1-kHz-wide spectral line. We control the field gradients  $\partial_z B_z$  and  $\partial_y B_z$  by adjusting the sum and the difference of small currents through parallel chip wires near the atoms (typically set-

ting  $\partial_y B_z = 0$ ). We directly calibrate the gradients by repeating spectroscopy measurements on a cloud translated by piezo-actuated mirrors on the trapping beams. The cloud position is measured using two orthogonal imaging systems, whose magnification is calibrated by a dropped  $^{87}\text{Rb}$  cloud in a magnetic-field-insensitive state. The systematic gradient uncertainty given in the main text is dominated by the magnification uncertainty.

### MAGNETIZATION MEASUREMENT

Magnetization decay is measured using a  $\pi/2 - \pi - \pi/2$  sequence. The first and second pulses have the same phase, but the final pulse has a variable relative phase  $\phi$ . Varying  $\phi$  reveals the magnitude of the transverse magnetization,  $|M_\perp|$ , in the visibility of the oscillation in relative population. We are sensitive to the relative frequency between the drive  $\omega$  and the atomic resonance  $\omega_0$ , with a precision of roughly  $1/t$ , where  $t$  is the hold time. For  $t \gtrsim 1$  ms, we find that our field stability (roughly 1 kHz, or a few parts in  $10^5$ ) is insufficient to preserve a reproducible relative phase throughout the sequence, resulting in a randomized phase for long hold times. To avoid an underestimation of the magnetization coherence time, we use the standard deviation of  $N_\uparrow/N_{\text{tot}}$  as a measure of  $|M_\perp|$ . Each measurement of  $|M_\perp|$  at a single hold time consists of 12 shots, ensuring sufficient sampling of the randomized phase. We find no systematic difference between  $\tau_M$  measured using rms and extremal values of the  $M_z$  distribution.

### STATE SELECTIVE IMAGING

Our imaging scheme allows us to simultaneously count the populations of atoms in states  $|\downarrow\rangle$  and  $|\text{p}\rangle$ , leaving atoms in state  $|\uparrow\rangle$  invisible. This is achieved with a Stern-Gerlach pulse to separate the trapped spin states, rf state manipulation during time-of-flight in a gradient, and finally, resonant absorption imaging on the  $|F = 9/2, m_F = -9/2\rangle$  to  $|F = 11/2, m_F = -11/2\rangle$  cycling transition. Imaging occurs after jumping the magnetic field to 209 G, the zero crossing of the s-wave scattering resonance, in order to minimize interaction effects during time of flight. In the magnetization measurements, we include an additional step transferring atoms in state  $|\uparrow\rangle$  to  $|\text{p}\rangle$  with an adiabatic rapid passage prior to imaging.

### TRANSVERSE DIFFUSIVITY OBSERVED IN 2D, REF. 10

Recent work by M. Koschorreck *et al.* shows a measurement of transverse spin diffusion in a strongly inter-

acting 2D Fermi gas that uses the same Zeeman states of  $^{40}\text{K}$  as does our present work [10]. Since the employed echo sequence is identical with the one used in our work, the model for the time evolution of the magnetization can be applied in full analogy and we expect (in our notation)  $M(t) \propto \exp[-t^3/(24\tau^3)]$ , with  $\tau = (2D_s^\perp \alpha^2)^{-1/3}$ . For the given Zeeman states  $\alpha \simeq 0.112 \mu_B/\hbar B' \simeq 981 \text{ kHz/G } B'$  at a magnetic field of 202.1 G, where  $\mu_B$  is the Bohr magneton. Figure 2a in Ref. [10] shows a magnetization trace with a decay time as defined above of  $\tau \simeq 6.5$  ms for a magnetic field gradient  $B' \simeq 4.7 \text{ G/cm}$  and  $\ln(k_F a) = -0.2$ , where  $a$  is the s-wave scattering length. For this curve, our analysis yields a spin diffusivity of  $D_{s,2\text{D}}^\perp \simeq 0.005 \hbar/m$  as opposed to  $0.25 \hbar/m$  stated. Although a correction had not appeared at the time of writing this manuscript, the authors of Ref. 10 concur with a missing factor of  $1/(2\pi)^2$  in the original analysis that yielded a minimum diffusivity  $D_{s,2\text{D}}^\perp = 0.25(3) \hbar/m$ .

### NORMALIZATION AND RESCALING OF RF SPECTRA

The rate of atom transfer from state  $|\uparrow\rangle$  to the weakly interacting probe state  $|\text{p}\rangle$  obeys the sum rule  $\int \Gamma(\omega) d\omega = \pi \Omega_R^2 N_\uparrow$ , where  $\Omega_R$  is the Rabi frequency of the applied rf pulse [24–27]. In the presence of strong interactions,  $\Gamma(\omega)$  scales as  $\Omega_R^2/(4\pi\sqrt{m/\hbar}\delta^{3/2})C$  for large positive detunings  $\delta = \omega - \omega_0$ , where  $\omega_0$  is the single-particle resonance frequency. We express the detuning in units of the Fermi energy,  $\Delta = \hbar\delta/E_F$ , where  $E_F$  is calculated for a balanced mixture with  $N = N_\sigma = N_{\text{tot}}/2$ . We furthermore introduce the normalized transfer rate  $\Pi(\Delta) = E_F/(\hbar\pi\Omega_R^2 N)\Gamma$  which obeys the sum rule  $\int \Pi(\Delta) d\Delta = 1$ . Its asymptotic behavior takes the form

$$\Pi(\Delta) \rightarrow \frac{1}{2^{3/2}\pi^2\Delta^{3/2}} \frac{C}{k_F N}, \quad (\text{S1})$$

and rescaling  $\Pi(\Delta)$  by  $2^{3/2}\pi^2\Delta^{3/2}$  reveals the contact per particle in units of  $k_F$ ,  $C/(k_F N)$ , as a constant asymptotic value for large  $\Delta$ .

In our experiments, we measure the fraction of atoms  $N_p/N$  transferred to the probe state by a Blackman pulse of length  $\Delta t$  and with mean Rabi frequency  $\Omega_R$ . We choose the rf power and pulse duration such that we probe the transition in the linear regime where  $\Gamma(\delta) = N_p(\delta)/\Delta t$ . Using the asymptotic behavior stated above, we obtain the contact from the fraction of atoms transferred, measured at a single detuning  $\delta$ , via

$$\frac{C}{k_F N} = \frac{4\pi}{\Omega_R^2 \Delta t} \delta^{3/2} \sqrt{\frac{m}{\hbar}} \frac{1}{k_F} \frac{N_p}{N}, \quad (\text{S2})$$

where the Fermi wave number  $k_F$  is calculated using the measured value for  $N = N_\uparrow$ .

## MAGNETIZATION DEPENDENCE OF THE CONTACT IN A NORMAL, SPIN-POLARIZED FERMION GAS

Here we consider the magnetization dependence of the contact density  $\mathcal{C}$  for a two-component gas of fermions described by the Hamiltonian

$$\mathcal{H} = \sum_{\sigma} \int d^3\mathbf{r} \psi_{\sigma}^{\dagger}(\mathbf{r}) \left( -\frac{\hbar^2 \nabla^2}{2m} - \mu_{\sigma} \right) \psi_{\sigma}(\mathbf{r}) + g \psi_{\uparrow}^{\dagger}(\mathbf{r}) \psi_{\downarrow}^{\dagger}(\mathbf{r}) \psi_{\downarrow}(\mathbf{r}) \psi_{\uparrow}(\mathbf{r}). \quad (\text{S3})$$

The chemical potentials  $\mu_{\sigma}$  are fixed by the constraint that the total density  $n$  and the (normalized) magnetization are kept constant.  $g \equiv [m/4\pi\hbar^2 a - \sum_{|\mathbf{k}| \leq \Lambda} m/(\hbar|\mathbf{k}|)^2]^{-1}$  is the coupling constant [32], regularized by the ultraviolet momentum cutoff  $\Lambda$ , and  $a$  is the  $s$ -wave scattering length. In our experiment,  $\mathbf{M}$  lies in the transverse plane. However, the interaction term is isotropic ( $s$ -wave scattering) and as a result, the contact density  $\mathcal{C}$ , being a scalar quantity, only depends on the magnitude of  $|\mathbf{M}|$ . Thus, in the discussion below, we take  $\mathbf{M} = M\hat{z}$ , without affecting the final conclusions.

A useful definition of the contact that makes clear its connection with interactions is [21]

$$\mathcal{C} = \langle g^2 \psi_{\uparrow}^{\dagger}(\mathbf{r}) \psi_{\downarrow}^{\dagger}(\mathbf{r}) \psi_{\downarrow}(\mathbf{r}) \psi_{\uparrow}(\mathbf{r}) \rangle. \quad (\text{S4})$$

This allows us to make the following observation: at sufficiently high temperatures, even though the interactions are strong in a gas near unitarity ( $a/\lambda_T \rightarrow \infty$ ;  $\lambda_T$  is the thermal de Broglie wavelength), many-body correlations are weak ( $\lambda_T \ll n^{-1/3}$ ) and (S4) can be factorized,

$$\mathcal{C}(M)/\mathcal{C}_0 = 1 - M^2, \quad (\text{S5})$$

where  $\mathcal{C}_0 \equiv \mathcal{C}(M=0)$  is the value of contact density at zero magnetization.

At lower temperatures,  $T \lesssim T_F$ ,  $\lambda_T$  is greater than the mean distance  $n^{-1/3}$  between atoms, and quantum many-body correlations become significant when the scattering length is large. In particular, pairing correlations associated with the formation of incoherent pairs above  $T_c$  are expected to modify the quadratic dependence of  $\mathcal{C}(M)/\mathcal{C}_0$  shown in (S5). We note, for instance, that for an ideal gas of dimer molecules – representing the BEC limit with maximal pairing correlations – with binding energy  $E_b = -\hbar^2/ma^2$ , the contact is  $\mathcal{C} = (4\pi n/a)(1-M)$ . Thus,

$$\mathcal{C}(M)/\mathcal{C}_0 = 1 - M. \quad (\text{S6})$$

It seems reasonable to expect that the incoherent pairs in a unitary Fermi gas in the regime  $T_c \lesssim T \lesssim T_F$  would give rise to a  $\mathcal{C}(M)/\mathcal{C}_0$  curve that is intermediate between the two extremes, (S5) and (S6).

One of the few techniques for treating such pairing effects systematically in the strong-interaction regime is the large- $\mathcal{N}$  expansion [33–35]. This approach artificially generalizes the  $\text{Sp}(2)$  quantum field theory (S3) of the dilute Fermi gas to an  $\text{Sp}(2\mathcal{N})$  theory with  $\mathcal{N}$  “flavors” of spin  $\uparrow$  and  $\downarrow$  fermions interacting via an  $\text{Sp}(2\mathcal{N})$ -invariant attractive interaction. The  $\mathcal{N} = \infty$  limit of this theory corresponds to the high-temperature “classical theory” in which (S5) is strictly satisfied; many-body quantum correlations are brought in via corrections in powers of  $1/\mathcal{N}$  and are expected to lead to deviations from (S5) at low temperatures.

To implement the large- $\mathcal{N}$  expansion, we write the grand canonical thermodynamic potential density  $\Omega$  as a functional integral over the Bose pairing field  $\phi$  [32, 34], where  $\beta \equiv (k_B T)^{-1}$ :

$$\Omega = -\beta^{-1} \ln \int \mathcal{D}[\phi^*, \phi] \exp \left\{ \mathcal{N} \int_0^{\beta} d\tau \int d^3\mathbf{r} \frac{|\phi(\mathbf{r}, \tau)|^2}{g} + \mathcal{N} \text{Tr} \ln[-\mathbf{G}^{-1}] \right\}. \quad (\text{S7})$$

Here the inverse matrix Nambu-Gor'kov Green's  $\mathbf{G}^{-1}$  function is [ $x \equiv (\mathbf{r}, \tau)$ ]

$$\mathbf{G}^{-1}(x, x') \equiv \begin{pmatrix} -\hbar\partial_{\tau} + \frac{\hbar^2 \nabla^2}{2m} + \mu_{\uparrow} & \phi(x) \\ \phi^*(x) & -\hbar\partial_{\tau} - \frac{\hbar^2 \nabla^2}{2m} - \mu_{\downarrow} \end{pmatrix} \delta(x - x'), \quad (\text{S8})$$

and the trace in (S7) is over space  $\mathbf{r}$ , imaginary time  $\tau$ , as well as matrix indices.

Using standard thermodynamic identities, one can rewrite Tan's “adiabatic relation” [36]  $\mathcal{C} = -(4\pi m/\hbar^2)(\partial\mathcal{E}/\partial a^{-1})_S$ , where  $\mathcal{E}$  is the energy

density and  $S$  is the entropy, as

$$\mathcal{C} = -\frac{m^2}{\hbar^4} \left( \frac{\partial\Omega}{\partial g^{-1}} \right)_{\mu_{\sigma}, T}. \quad (\text{S9})$$

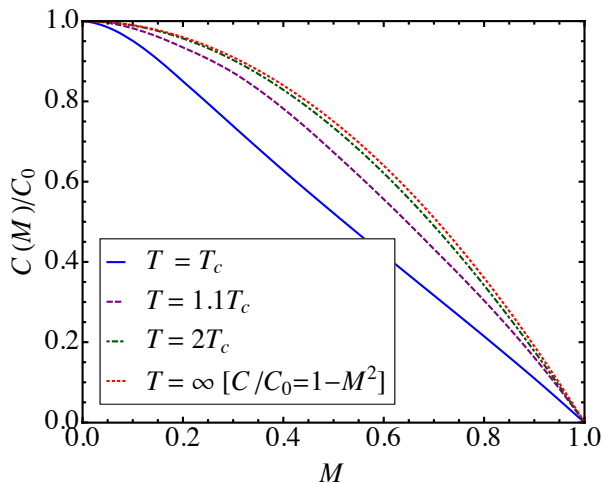


FIG. S1. Magnetization dependence of the contact in a normal unitary Fermi gas to leading order in a large- $\mathcal{N}$  calculation at various temperatures, scaled by  $\mathcal{C}(M=0)$ . Deviations from the high- $T$  asymptote  $\mathcal{C}(M)/\mathcal{C}_0 = 1 - M^2$  in the region above  $T_c$  signal the onset of strong pairing correlations.

Applying this to (S7) (with  $\mathcal{N} = 1$ ), it is immediately apparent that the contact is just the expectation value of the square of the amplitude of the Bose pairing field:  $\mathcal{C} = (m^2/\hbar^4\beta) \int_0^\beta d\tau \int d^3\mathbf{r} \langle |\phi(\mathbf{r}, \tau)|^2 \rangle$ . Formally, this is an exact identity. To make progress, however, we need to expand the argument of the exponential in (S7) to order  $1/\mathcal{N}$  (i.e., Gaussian with respect to  $\phi$ ). In the normal state ( $\langle \phi \rangle = 0$ ) above  $T_c$ , Fourier transforming to momentum  $\mathbf{q}$  and Matsubara frequency  $\nu_m$  space, the  $\mathcal{O}(1/\mathcal{N})$  contribution to the thermodynamic potential is [32]

$$\Omega = -\frac{1}{\beta} \ln \int \mathcal{D}[\phi^*, \phi] \exp \left[ \mathcal{N} \sum_{\mathbf{q}, \nu_m} \frac{1}{\Gamma}(\mathbf{q}, i\nu_m) |\phi(\mathbf{q}, i\nu_m)|^2 \right] \quad (\text{S10})$$

and hence (there is no  $\mathcal{O}(1/\mathcal{N})^0$  contribution in the nor-

mal state since  $\langle \phi \rangle = 0$ ) [35],

$$\mathcal{C} = \frac{m^2}{\hbar^4\beta\mathcal{N}} \sum_{\mathbf{q}, \nu_m} \Gamma(\mathbf{q}, i\nu_m) + \mathcal{O}(1/\mathcal{N})^2. \quad (\text{S11})$$

Here the two-particle vertex function  $\Gamma$  is defined by its inverse

$$\Gamma^{-1}(\mathbf{q}, i\nu_m) = \frac{1}{g} - \sum_{\mathbf{k}} \frac{1 - f(\xi_{\mathbf{k}\uparrow}) - f(\xi_{\mathbf{k}\downarrow})}{\hbar i\nu_m - \xi_{\mathbf{k}\uparrow} - \xi_{\mathbf{k}+\mathbf{q}\downarrow}}. \quad (\text{S12})$$

$f(\xi_{\mathbf{k}\sigma})$  is the Fermi-Dirac distribution for spin  $\sigma$  and  $\xi_{\mathbf{k}\sigma} \equiv \hbar^2|\mathbf{k}|^2/2m - \mu_\sigma$ . Since (S11) is already order  $1/\mathcal{N}$ , the chemical potentials that enter the two-particle vertex function can be obtained from the  $\mathcal{O}(1/\mathcal{N})^0$  mean-field number equations  $n = \sum_{\mathbf{k}} [f(\xi_{\mathbf{k}\uparrow}) + f(\xi_{\mathbf{k}\downarrow})]$  and  $M = \sum_{\mathbf{k}} [f(\xi_{\mathbf{k}\uparrow}) - f(\xi_{\mathbf{k}\downarrow})]/n$ .

Solving (S11) and (S12) in conjunction with the mean-field number equations at unitarity gives the contact as a function of magnetization shown in Figure S1 for several values of  $T/T_c$ . To leading order in  $1/\mathcal{N}$ , the critical temperature where the pairing susceptibility diverges,  $\Gamma(\mathbf{0}, 0) = \infty$ , is the mean-field value,  $T_c \sim 0.5T_F$ . At high-temperatures  $T \gg T_c$ , where the fugacities  $z \equiv \exp(\beta\mu_\sigma)$  are small, it is straightforward to show that (S11) and (S12) reduce to  $\mathcal{C}(M, \beta\mu_\sigma \ll 0) = (16\pi z_\uparrow z_\downarrow)/\lambda_T^4$ . Using the high- $T$  limits  $n\lambda_T^3 \rightarrow z_\uparrow + z_\downarrow$  and  $Mn\lambda_T^3 \rightarrow z_\uparrow - z_\downarrow$  of the number equations, this gives

$$\mathcal{C}(M, \beta\mu_\sigma \ll 0) = 4\pi n^2 \lambda_T^2 (1 - M^2), \quad (\text{S13})$$

in agreement with the expected high- $T$  asymptote (S5) as well as the leading order virial expansion value of the contact at zero magnetization [37]. From Figure S1, we see that the contact saturates to this asymptotic  $1 - M^2$  behavior already at only moderately high temperatures,  $T \sim 2T_c$ . Quantum corrections are only evident at lower temperatures, where strong enhancement of the pairing susceptibility leads to a suppression of  $\mathcal{C}(M)/\mathcal{C}_0$ , suggestive of the pairing behavior responsible for (S6). This effect is seen as well in Figure 4(d) in the main text although our simple calculation here likely underestimates the range of temperatures above  $T_c$  where this effect is evident.